PCCP

Cite this: *Phys. Chem. Chem. Phys.*, 2011, **13**, 15666–15672

www.rsc.org/pccp

PAPER

X-Ray spectra and electronic correlations of $FeSe_{1-x}Te_x$

C. L. Chen,*[a] C. L. Dong,*[b] J. L. Chen,[cd] J.-H. Guo,[c] W. L. Yang,[c] C. C. Hsu,[b] K. W. Yeh,[a] T. W. Huang,[a] B. H. Mok,[a] T. S. Chan,[b] J. F. Lee,[b] C. L. Chang,[d] S. M. Rao[a] and M. K. Wu[a]

Received 15th March 2011, Accepted 12th July 2011
DOI: 10.1039/c1cp20765b

Critical issues concerning emerging Fe-based superconductors include the degree of electron correlation and the origin of the superconductivity. X-Ray absorption spectra (XAS) and resonant inelastic X-ray scattering spectra (RIXS) of $FeSe_{1-x}Te_x$ (x = 0–1) single crystals were obtained to study their electronic properties that relate to electron correlation and superconductivity. The linewidth of Fe $L_{2,3}$-edges XAS of $FeSe_{1-x}Te_x$ is narrower than that of Fe–pnictides, revealing the difference between their hybridization effects and localization character and those of other Fe–pnictides. While no significant differences exist between the Fe L-edge XAS and RIXS of $FeSe_{1-x}Te_x$ and those of Fe–pnictides, Se K-edge and Te K-edge XAS exhibit substantial edge shift, suggesting that the superconductivity in an Fe–Se superconductor is strongly associated with the ligand states. A comparison of the Se K-edge and Te K-edge spectra reveals that the charge transfer may occur between Se and Te. Given the Coulomb interaction and the bandwidth, the spectral results indicate that $FeSe_{1-x}Te_x$ is unlikely to be a weakly correlated system unlike the Fe–pnictides of the "1111" and "122" families. The spectral results further demonstrate that superconductivity in this class of Fe-based compounds is strongly associated with the ligand 4p hole state.

Introduction

High-temperature superconductivity has been discovered in Fe-based quaternary oxypnictides. This is the first system in which Fe is crucial for superconductivity.[1] Usually Fe has magnetic moments and tends to form an ordered magnetic state. Neutron-scattering experiments have demonstrated that mediated superconducting pairing may be caused by magnetic fluctuations, in a manner similar to that in high-T_c cuprates.[2,3] The binary superconductor FeSe is another example of an Fe-based superconductor;[4] T_c of FeSe is ~8 K and depends on the composition such that T_c decreases with over-doping or under-doping of compounds,[5] as does that of high-T_c cuprates. FeSe has attracted considerable interest because of its simple tetragonally symmetric $P4/nmm$ crystalline structure, comprising a stack of layers of edge-sharing $FeSe_4$ tetrahedron. This binary system is isostructural with the FeAs layer in quaternary iron arsenide, suggesting that this simple binary compound may provide valuable information to help elucidate the origin of high-temperature superconductivity in Fe-based compounds. Band-structure calculations indicate that FeSe- and FeAs-based compounds have similar Fermi-surface structures,[6] but the making of spectral measurements of pure FeSe is hindered by the poor quality of crystals that arise from serious oxidization at their surfaces. Therefore investigation of the effect of chemical substitution, at either Se or Fe sites, is warranted to maintain or to improve superconducting behavior on the one hand and to stabilize the crystalline structure on the other. Te doping of the layered FeSe with the PbO structure modifies its superconducting behavior, with a maximum T_c of ~15 K when Te replaces half of the Se. The enhancement of T_c that is correlated with the structural distortion that results from Te substitution is attributed to the combined effect of lattice disorder, arising from the substitution of larger ions, and electronic interaction. Since layered $FeSe_{1-x}Te_x$ crystals are readily cleaved and highly crystalline, clearer information about the electronic structure can be obtained from X-ray spectra of layered $FeSe_{1-x}Te_x$ crystals than from those of FeSe crystals. Hence, X-ray absorption (XAS) and resonant inelastic X-ray scattering (RIXS) were used to investigate the electronic properties of $FeSe_{1-x}Te_x$ (x = 0–1) single crystals. XAS is a powerful tool for probing the crystal field and electronic interactions. The excitation-induced energy-loss features in RIXS can be viewed as an indicator of the strength of the electron correlation.

[a] *Institute of Physics, Academia Sinica, Taipei 11529, Taiwan. E-mail: clchen@phys.sinica.edu.tw*
[b] *National Synchrotron Radiation Research Center, HsinChu 30076, Taiwan. E-mail: dong.cl@nsrrc.org.tw*
[c] *Advanced Light Source, Lawrence Berkeley National Laboratory, Berkeley, CA, USA*
[d] *Department of Physics, Tamkang University, Tamsui, Taipei County, Taiwan*

Based on related experimental and theoretical work on Fe–pnictides, Yang *et al.*[7] explicated basic physical issues related to Fe-based quaternary oxypnictides, but few Fe–Se samples of this class were investigated spectroscopically. An angle-resolved photoemission combined with a DFT band structure calculation for an "11" Fe-based superconductor $FeSe_{0.42}Te_{0.58}$ reveal effective carrier mass enhancement, which is characteristic of a strong electronic correlation.[8] This finding is supported by the large Sommerfeld coefficient, ~39 mJ mol^{-1} K^{-2},[9] and reveals that the FeSe "11" system is a strongly correlated system and its electronic correlation differs substantially from that of the "1111" and "122" compounds, perhaps because of the subtle differences between the p–d hybridizations in the Fe–pnictides and the FeSe "11" system. This argument is consistent with the observation of p–d hybridization herein. This claim is also supported by recent DMFT calculations, which demonstrate that correlations are overestimated mainly because of the incompleteness of the understanding of the hybridization between the Fe d and pnictogen p states.[10] Nakayama *et al.* discussed the pairing mechanism based on interband scattering, which has a signature of the Fermi surface nesting in ARPES. Their estimates, based on the SC gap value, suggest that the system is highly correlated.[11] Moreover, a combined electron paramagnetic resonance (EPR) and NMR study of the $FeSe_{0.42}Te_{0.58}$ superconductor has indicated the coexistence of electronic itinerant and localized states.[12] The coupling of the intrinsic state with localized character to itinerant electrons exhibits some similarities with the Kondo effect, which is regarded as typical interaction of a strongly correlated electron system. The localized state is characteristic of strong electron correlations and makes the FeSe "11" family a close relative of high-T_c superconductors. Based on a direct comparison of the XAS and RIXS spectra, we suggest that $FeSe_{1-x}Te_x$ is unlikely to be a weakly correlated system, and so differs from other Fe-based quaternary oxypnictides. The charge transfer between Se–Te and the Se 4p hole state that is induced by the substitution is strongly correlated with the superconducting behavior. All of these results suggest strong electronic correlations in the FeSe "11" system.

Experiments

Large layered single crystals of high-quality $FeSe_{1-x}Te_x$ were grown using an optical zone-melting growth method. Elemental powders of $FeSe_{1-x}Te_x$ were loaded into a double quartz ampoule, which was evacuated and sealed. The ampoule was loaded into an optical floating-zone furnace in which 2×1500 W halogen lamps were installed as sources of infrared radiation. The ampoule moved at a rate of 1.5 mm h^{-1}. As-grown crystals were subsequently homogenized by annealing at 700–800 °C for 48 h, and at 420 °C for another 30 h. Chemical compositions of $FeSe_{1-x}Te_x$ single crystals were determined by energy-dispersive X-ray analysis (EDX). The actual composition of nominal $x = 0.3$ was $FeSe_{0.56}Te_{0.41}$; that of nominal $x = 0.5$ was $FeSe_{0.39}Te_{0.57}$; that of nominal $x = 0.7$ was $FeSe_{0.25}Te_{0.72}$ and that of nominal $x = 1.0$ was $FeTe_{0.91}$. The quality of the sample was evaluated by X-ray powder diffraction; T_c was confirmed by both transport and magnetic measurements.[13]

XAS was adopted to probe the unoccupied partial density of states of the conduction band, while XES was utilized to obtain complementary information to that obtained by XAS. The results thus obtained reveal the occupied partial density of states associated with the valence band. Tuning the incident X-ray photon energies at resonance in XAS yields the RIXS spectrum, which is used primarily to probe the low-excited energy-loss feature which is symptomatic of the electron correlation. Detailed X-ray absorption and emission studies were conducted as follows. The Se and Te K-edge XAS were recorded at beamline BL01C at the National Synchrotron Radiation Research Center (NSRRC) in Hsinchu, Taiwan, operated at 1.5 GeV with a current of 360 mA. The resolving power of this beamline is better than $\Delta E/E \sim 2 \times 10^{-4}$. All spectra were normalized to unit step height in the absorption coefficient from well below to well above the edges and yield the information of the unoccupied states with p character. XAS and XES measurements of the Fe $L_{2,3}$-edges were made at beamlines 7.0.1 and 8.0 at Advanced Light Source (ALS) at Lawrence Berkeley National Laboratory (LBNL). In the Fe L-edge X-ray absorption process, the electron in the Fe 2p core level was excited to the empty 3d and 4s states, and the XES spectra were then recorded as the signal associated partial densities of states with Fe 4s as well as Fe 3d character. The RIXS spectra were obtained by properly selecting various excitation energies to record the XES spectra, based on the X-ray absorption spectral profile. The XAS spectra were obtained with an energy resolution of 0.2 eV by recording the sample current. The X-ray emission spectra were recorded using a high-resolution grazing-incidence grating spectrometer with a two-dimensional multi-channel plate detector with the resolution set to 0.6 eV.[14] Surface oxidization is a serious issue for Fe-based superconductors; to prevent oxidation of the surface, all data were collected on a surface of the sample that was cleaved *in situ* in a vacuum environment with a base pressure of 2.7×10^{-9} torr.

Results and discussion

Fig. 1(a) compares Fe $L_{2,3}$-edges XAS spectra of $FeSe_{1-x}Te_x$ before and after cleavage *in situ* and an oxidized iron foil is used as a reference sample. Of two XAS lines, A_1 and B_1, at the L_3-edge of the oxidized iron foil, B_1 is prominent from the uncleaved samples, indicating that contamination of the sample surface by oxygen is a serious issue. The shoulder-like line B_1, which arises from Fe–O bonding in cleaved samples, is smeared. Iron oxide is well known to yield B_1, but this line is absent from the spectra of cleaved $FeSe_{1-x}Te_x$ samples, indicating that iron oxide is only a very minor constituent. This effect demonstrates the importance of cleavage *in situ* for making spectral measurements of samples in this class. Fig. 1(b) presents Fe $L_{2,3}$-edges XAS spectra of $FeSe_{1-x}Te_x$, using Fe metal, oxidized foil and Fe_2O_3 as reference samples. XAS was used to probe unoccupied Fe 3d orbitals. The spectra reveal two major transitions. Governed by the dipole selection rule, the transition is mainly due to $2p^63d^6$–$2p^53d^7$ transition, in which an Fe 2p electron is excited into an empty

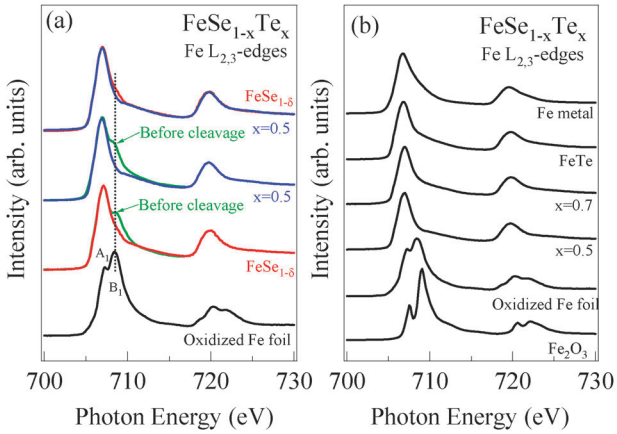

Fig. 1 (a) Comparison of Fe $L_{2,3}$-edge XAS of $FeSe_{1-x}Te_x$ before and after cleavage *in situ*, using an oxidized iron foil as reference. (b) Fe $L_{2,3}$-edge XAS of $FeSe_{1-x}Te_x$ cleaved *in situ*. Samples of Fe metal, oxidized foil and Fe_2O_3 serve as references.

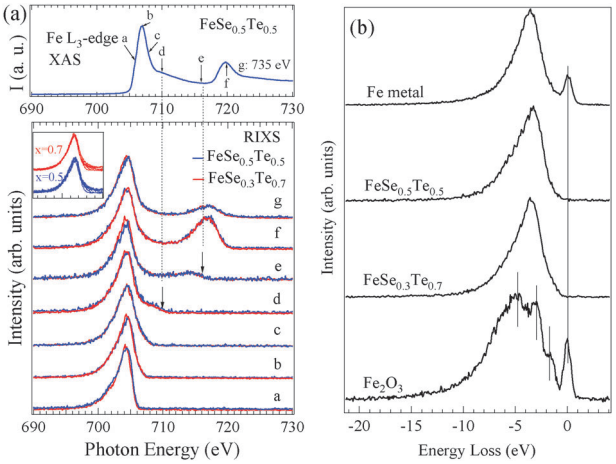

Fig. 2 (a) RIXS (lower part) obtained at selected energies (a–g) that are indicated by arrows in XAS (upper part). Inset shows fluorescent feature of both samples, which overlaps well with the line at 704 eV in the non-resonant spectrum. (b) Comparison of RIXS resonantly excited at 708 eV for samples with $x = 0.5$ and 0.7 and reference samples Fe_2O_3 and pure iron metal.

3d state. Spin–orbit splitting separates the 2p state into $2p_{3/2}$ and $2p_{1/2}$ states, yielding two prominent absorption features around 707 eV (L_3) and 720 eV (L_2). XAS at the transition-metal L-edge probed unoccupied 3d states that are sensitive to the chemical environment, valence state, crystal field and 3d electronic interactions. The ratio of intensities of the two major absorption features is largely determined by the high- or low-spin ground states through the crystal-field effect. XAS of Fe_2O_3 reveals a strongly split structure at both L_2 and L_3 absorption edges, which is formed by the interplay of crystal field and electronic interactions. Fe–O makes no contribution to the $FeSe_{1-x}Te_x$ spectra, and no spectral profile resembles that of Fe_2O_3 or oxidized foil. The shoulder at the high-energy tail (dotted part) of the Fe L_3 line in the $FeSe_{1-x}Te_x$ samples is thought to be associated with covalent sp^3 bonds between Fe 3d and Se 4p/Te 5p states.[15] $FeSe_{1-x}Te_x$ yielded no observable line splitting or change in intensity ratio, implying a weak crystal-field effect and that the Fe ion favors a high-spin ground state. The line shapes in the spectra of these cleaved crystals in the UHV chamber resemble those of iron metal, indicating metallicity and a localized 3d band.[7] The variation in the full width at half maximum (FWHM) of the Fe L_3 peak in the XAS and the width of the Fe 3d band with localized character are expected to be smaller than those of Fe because the Fe–Fe interaction is stronger.[16]

Fig. 2(a) presents the RIXS (lower part) obtained at selected energies (letters a–g) that are indicated by arrows in the XAS (upper part). The upper RIXS spectrum was obtained at an excitation photon energy of 735 eV—far above the Fe L_3-edge absorption threshold. This spectrum is known as the so-called non-resonant normal emission spectrum. This non-resonant spectrum shows two main fluorescent features around 704 eV and 717 eV, resulting from de-excitation transitions from occupied 3d states to the $2p_{3/2}$ and $2p_{1/2}$ holes, respectively, which are thereby refilled. The RIXS that were recorded with various excitation energies, a–f, include the strong 704 eV peak, as seen in the non-resonant spectrum. At an excitation energy close to that of the L_2 absorption feature, the line at 717 eV emerges and remains at the same energy as the excitation energy increases beyond the L_2 edge. Indicated by arrows in spectra d and e, small bumps appeared at energies of approximately 710 and 716 eV. These energies track well the excitation energies and are therefore caused by elastic scattering. Magnified in the inset, the fluorescent feature of both samples does not follow the excitation energy and overlaps well the line at 704 eV in the non-resonant spectrum. The RIXS included no energy loss feature, which is generally associated with electron correlation and excitations.

Fig. 2(b) compares RIXS that were obtained with resonant excitation at 708 eV from samples with $x = 0.5$ and 0.7 and from reference samples Fe_2O_3 and pure iron metal. They are displayed with an energy loss scale; the feature at an energy loss of zero is produced by elastic scattering. The Fe_2O_3 RIXS exhibit more complicated energy-loss features, which are marked by short vertical lines. These features were enhanced at particular excitation energies because of inter-electronic transitions, and are identified as d–d excitations.[17] Fe metal yields one main fluorescent line and a more symmetric profile. Spectra of $FeSe_{1-x}Te_x$ are also clearly dominated by only a single line and resemble that of Fe metal, implying metallic character. The absence of excitation-induced energy-loss features in RIXS of iron–pnictide samples, according to an analysis of the coulombic interaction and Fe 3d bandwidth, may imply a weak correlation in the iron–pnictide system.[7] A further comparison with known metallic iron and insulating iron oxide must thus be made to reveal the importance of electron correlation and metallicity.

Just as XAS demonstrates the density of unoccupied states (DOS) in d orbitals, non-resonant XES are simply interpreted as revealing the occupied DOS of d states, which is dominated by Fe 3d orbitals near the Fermi level. Fig. 3(a) shows the non-resonant Fe $L_{2,3}$-XES of Fe_2O_3, $FeSe_{1-x}Te_x$ and Fe metal. The spectra of $FeSe_{1-x}Te_x$ and Fe are almost identical in both shape and energy indicating that the experimental determination of the contribution of occupied Fe 3d states in $FeSe_{1-x}Te_x$ is similar to that of Fe metal. The ratio of intensities of L_2 and L_3 XES should be equal to 1/2 for free atoms,

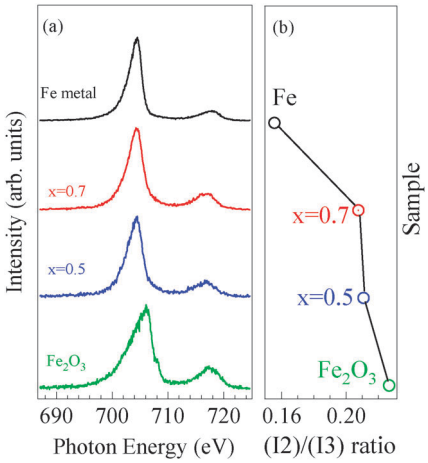

Fig. 3 (a) Comparison of non-resonant Fe $L_{2,3}$-XES of Fe_2O_3, $FeSe_{1-x}Te_x$ and Fe metal. (b) Ratio of integrated intensities (I_2/I_3) of XES L_2 and L_3 lines.

reflecting the statistical populations of the $2p_{1/2}$ and $2p_{3/2}$ energy levels, but in metals, Coster–Kronig transitions greatly reduce this ratio, revealing the correlations and metallicity of a system.[18] Fig. 3(b) presents the ratio I_2/I_3, which is the ratio of integrated intensities of the XES L_2 and L_3 lines. $FeSe_{1-x}Te_x$ samples with $x = 0.5$ and $x = 0.7$ have almost identical I_2/I_3 intensity ratios. These ratios are closer to that of correlated Fe_2O_3 than to that of the metal, indicating that the character of $FeSe_{1-x}Te_x$ is more like that of correlated Fe_2O_3. This finding is consistent with the Fe 3d states in $FeSe_{1-x}Te_x$ systems, which exhibit more localized than itinerant character, as revealed by a smaller FWMH in XAS than that of Fe–pnictides.

The similarity between the XAS and XES of $FeSe_{1-x}Te_x$ and those of Fe metal signifies the importance of metallicity in this system. This metallicity is further and directly ascertained from absorption–emission spectra, which, with a carefully calibrated energy scale, can reveal both the occupied and the unoccupied electronic densities of states around the Fermi level. Fig. 4(a) displays the absorption–emission spectra, revealing the DOS of Fe 3d states across the Fermi level. An arrow indicates the intersection of XAS and XES and indicates that $FeSe_{1-x}Te_x$ can be regarded as metallic. Fig. 4(b) shows overlain spectra of $FeSe_{1-x}Te_x$ and Fe. The Fe spectrum has a single line, which is narrower than the corresponding line of $FeSe_{1-x}Te_x$. This dominant line in the spectrum of $FeSe_{1-x}Te_x$ is slightly broader than that from Fe, perhaps because of an Se hybridization state in the lower-energy region.[19,20]

Iron–pnictides are weakly correlated systems, unlike high-T_c cuprates. However, theoretical work has established that Fe–Se may not be correlated as weakly as Fe–pnictides.[21] An important question that arises concerns whether compounds in the FeSe family exhibit a weak correlation, like that of iron–pnictides, or a strong correlation, like that in high-T_c cuprates. The key to this matter is to obtain information concerning the bandwidth of the Fe 3d states from spectral results. An estimate of the FWHM in $FeSe_{1-x}Te_x$ XES yields a width of 4.1 eV. This value reflects the fact that core–hole lifetime and multiplet broadening are not associated with the Fe 3d bandwidth. Fig. 4(c) presents a deconvoluted

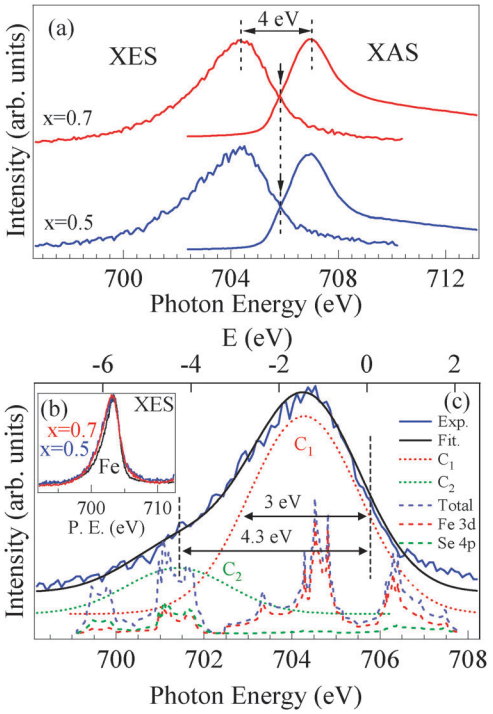

Fig. 4 (a) Absorption–emission spectrum of $FeSe_{1-x}Te_x$ ($x = 0.5$ and 0.7). Intersection yield indicates E_F. (b) Spectra of $FeSe_{1-x}Te_x$ ($x = 0.5$ and 0.7) and Fe metal. Deviation arises from Fe–Se hybridized states. (c) Fe L_3-XES line is fitted by two components (dotted lines). The dashed lines refer to calculated DOS (from ref. 19).

spectrum that includes a single dominant line (C_1) and a low-energy contribution (C_2) that is consistent with published X-ray data.[22] The main line is associated primarily with Fe 3d bands;[23] the contribution in the low-energy region is interpreted as resulting from hybridization of Fe 3d and Se 4p states. The low-energy shoulder has been understood to originate from hybridization of Fe 3d and As 4p states in the FeAsFO "1111" system. The results concerning the FeSe "11" system reveal that it is simpler than the "1111" system: the low-energy contribution is from hybridization of Fe 3d–Se 4p without calculation prediction. This hybridization of Fe 3d–Se 4p is also consistent with recent density functional calculations.[19] As seen in the projected density of states (adopted from ref. 19) in the bottom of Fig. 4(c), the peak C_1 is mainly due to the Fe 3d states. The peak C_2 lies far below the Fermi level and can be ascribed to the hybridized Fe 3d–Se 4p states. The width of the dominant peak in the Fe L_3 XES is $\sim$3 eV. Given the instrumentation resolution, this value is taken as a guide for an upper limit of the Fe 3d bandwidth. The estimate of $\sim$3 eV for the Fe 3d bandwidth agrees with the on–off-resonance photoemission results, which reveal that Fe dominates the binding energy range 0–3 eV.[20] The low-energy contribution at 4.3 eV below E_F is attributed to Se 4p states, consistent with the on–off-resonance photoemission results[20] and DOS calculation.[19] The degree of electron correlation simply implies the relative magnitudes of the Coulomb interaction U and bandwidth W. U is simply taken as the energy difference between the occupied and unoccupied states near E_F, and is estimated to be $\sim$4 eV. This value matches values presented in other work, in which U of the FeSe system

has been predicted to be ~4 eV.[21] The values imply that the magnitude of U is larger than that of the upper limit of the estimated Fe 3d bandwidth. The result $U/W > 1$ in this study reflects a strong electronic correlation due to competition between the localized effect of U and the itinerant character of W.[24]

To elucidate electron correlation in these Fe-based compounds, various experiments and theoretical calculations have been conducted, especially for the "1111" and "122" systems. Now, the results herein concerning the "11" system are compared to those obtained elsewhere for "1111" and "122" compounds. A comparison of the photoemission spectrum (PES) of Fe with the Cu 2p core-level spectra of $CeFeAsO_{0.89}F_{0.11}$ (1111)[15] and high-T_c cuprates ($La_{2-x}Sr_xCuO_4$ and $Nd_{2-x}Ce_xCuO_{4-\delta}$)[25] reveals the absence of satellite structures with higher binding energies in the Fe 2p spectra, which implies the presence of strongly itinerant Fe 3d electrons, which contrasts with the observation from the Cu 2p spectra in high-T_c cuprates. A further comparison of the Fe L_3 XAS spectra shows the absence of a well-defined multiplet structure, which is indicative of the delocalization of 3d band states, providing complementary evidence of the itinerant character of Fe 3d electrons. Strongly itinerant 3d electrons are therefore an important characteristic of the Fe-based superconductor, implying that it does not exhibit as strong correlations as high-T_c cuprates. The degree of electron correlations in PrFeAsO has been examined by coupled X-ray absorption and emission spectroscopy.[22] From the spectroscopic results herein, the bandwidth of the Fe 3d states is estimated to be ~2eV, which is similar to or larger than the theoretical Coulomb parameter $U \leq 2$ eV. The relative magnitudes of U and W thus simply suggest that the "1111" system exhibits weak to intermediate electron correlations.[22] A detailed study that involves the theoretical calculations for both "1111" and "122" Fe–pnictides has been performed and its results are highly consistent with experimental X-ray spectroscopic results.[7] A cluster calculation was conducted to highlight the role of strong Coulomb correlations; spectral features that are associated with strong correlations are shown in the theoretical results, but are suppressed in the experimental data. Based on a direct comparison of the energy position of this feature in the experimental data and that in the cluster simulation, an upper limit of the Hubbard U of 2 eV is determined; this value is markedly smaller than the Fe 3d bandwidth. This result suggests that Fe–pnictides should be viewed as a weakly correlated system. Although the XAS results herein are similar to previously obtained XAS results for Fe–pnictides and do not show the well-defined multiplet structure that is exhibited by Fe ionic oxides, two important differences are observed under the close inspection: (a) the high-energy shoulder intensity of $FeSe_{1-x}Te_x$ is lower than that of Fe–pnictides, and (b) the linewidth of the main peak in the XAS spectrum of Fe metal is smaller than that of Fe–pnictides.[7] The weak and broad shoulder is the result of hybridization of Fe 3d–Z np states (Z: sp element). Thus this reduction in intensity implies less hybridization than exhibited by other Fe-based "1111" and "122" systems. This finding is consistent with the observation that the linewidth of the Fe 3d main peak from FeSe is narrower than those from the "1111" and "122" systems. The presence of localized Fe 3d electrons in the FeSe system is also confirmed by XES, which can be used to extract information about the bandwidth of the Fe 3d states. The bandwidth in this study was estimated to be ~3 eV, although this value is larger than that, ~2 eV, found in a previous study of the "1111" system.[15] However, from the spectroscopic results herein, the Coulomb parameter U is estimated to be ~4 eV, which exceeds values reported elsewhere, which range from 0.8 eV to 2 eV.[7,15,16] The Coulomb parameter U ~4 eV herein is also supported by recent calculation studies. These differences suggest that the FeSe system differs from "1111" and "122" compounds, and the FeSe "11" system is probably not a weakly correlated system.

The electronic properties discussed above concern Fe 3d orbitals. The correlation between the superconducting behavior and the band structures, as well as interaction of the d–d and d–p states, may also be important in these systems, as revealed by the XANES tests on $FeSe_{1-x}$ single crystals.[26] The electronic configuration depends strongly on the hybridization between the orbitals of the Fe (3d)–Se(4p)/Te(5p) states. Accordingly, the electronic properties of the 4p(5p)-character, which are identified from the Se (Te) K-edge XAS spectra, must be further investigated. The Fe K-edge spectral profiles of the $FeSe_{1-x}Te_x$ are identical and seem to be unaffected by Te doping (not shown here), consistent with observations of Fe L-edge XAS and RIXS, implying that the valence state and the electronic structure around the iron sites are similar. Fig. 5(a) and (b) display the Se and Te K-edge spectra, respectively. The insets highlight the energy shifts in these spectra. Se K-edge spectra have a spectral line shape similar to that in our earlier investigation.[26] The spectra are explained by a projection to the local electronic transition from the Se inner 1s to the outer 4p state. The spectra exhibit two peaks A_2 and B_2. The peak A_2 at a photon energy of around 12 658 eV results from Fe–Se hybridized states. The peak of the doped sample has increased intensity and is shifted to higher energy. According to the discussions elsewhere,[26,27] the increase in the intensity of peak A_2 is caused by an increase in the strength of Fe 3d–Se 4p hybridization. The shift upward in energy is the result of an increase in the valence states. The measured energies of the absorption edge followed the order of increasing photon energy $x = 0.3$, 0.7 and 0.5, as displayed in the inset. Fig. 6 plots the values. The position of the absorption

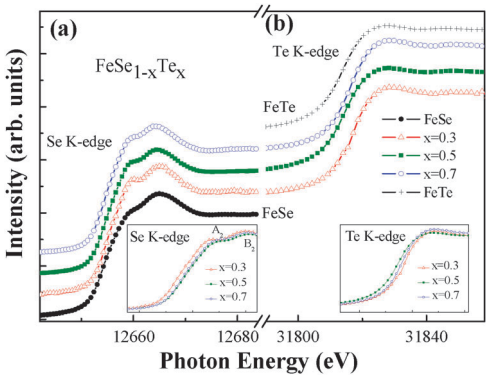

Fig. 5 XAS of (a) Se K-edge and (b) Te K-edge. Insets show details of energy shifts of (a) Se K and (b) Te K-edge upon Te doping.

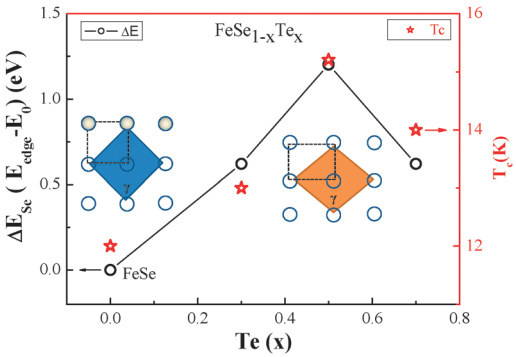

Fig. 6 Energy shift of Se K-edge (black circle) and T_c as functions of Te doping. Sketch of variation of angle γ also shown.

edge is related to the valence state; the valence state is highest at $x = 0.5$, implying that the carriers between the Fe and Se are itinerant electrons in the Fe–Se hybridization band, causing a valence change upon Te substitution. This increase in the valence is an indication of the change in coordination geometry and the increase in the number of 4p holes. The spectra thus provide evidence that the 4p holes are most increased upon Te substitution when $x = 0.5$. The change in the number of holes that is caused by the variation in the strength of the Fe 3d–Se 4p hybridization band is also evidenced by the X-ray absorption study of the Se deficiencies in the FeSe system.[26] The number of holes changes with the superconductivity (Fig. 6) in a manner similar to that in cuprate, whose itinerant holes, *via* the hybridization of Cu 3d–O 2p states, are responsible for superconductivity. Consequently, the change in valence implies a change in the number of holes by Fe 3d–Se 4p hybridization, forming itinerant holes, as occurs in Se-deficient FeSe. The broad feature B_2 appears around 20 eV above the absorption threshold in all spectra. According to Chen *et al.*[26] and Joseph *et al.*,[27] this feature is attributed to multiple scatterings from the symmetrical Se 4p states in the coordination sphere that is related to the local structure of the Se site. This broad feature appears at the same energy in all of the $FeSe_x$ spectra and is unaffected by the Se deficiency.[26] This finding indicates similar multiple scattering from Se 4p states and the same local structure around Se ions. However, this broad feature does not occur at the energy at which it occurred in the work of Joseph *et al.*,[27] because of the change in the local geometry around the Se site upon Te substitution, suggesting local inhomogeneity, which is consistent with the local inhomogeneity that was evident in XANES[27] and EXAFS[28] studies. An analysis of the EXAFS results reveals that the Fe–Se and Fe–Te bond lengths in $FeSe_{0.5}Te_{0.5}$ differ, revealing distinct site occupation and local inhomogeneity. A detailed polarization study of the Se K-edge demonstrated changes in the A_2 and B_2 peaks with the *xy* and *z* character of the p states:[27] because of the natural character of the p orbitals, the multiple scattering in the XAS results that is associated with p orbital symmetry reveals their different orbital orientations, and so reflects p_{xy} and p_z character. This feature shifted to lower energy as a result of the local inhomogeneity that is caused by doping. This finding is supported by the work of Joseph *et al.*,[27] and implies distortion of the tetrahedral symmetry at the Se sites. Te K-edge spectra in Fig. 5(b) include one edge feature that is associated with 1s to 5p transitions in the coordination sphere, which reflect the local envelopment of the Te ions. The inset in Fig. 5(b) presents details of the absorption edge. The photon energy associated with the chemical shifts increases in the order $x = 0.5$, 0.7 and 0.3, which trend opposes the Se K-edge observations. The $x = 0.5$ substitution exhibits the lowest valence state, which finding contrasts with the Se K-edge results, possibly that charge is gained in the 5p orbital at the Te site. The critical and corresponding energy shift in the Se and Te K-edge features upon Te substitution is consequently indicative of an increase in the 4p holes and a decrease in the 5p holes at $x = 0.5$. The tetragonal phase of FeSe has a planar sub-lattice layered structure with Se ions at the tips of the pyramid chain and an Fe plane between Se ions. The substituted Te has an ionic radius which exceeds that of Se, and so increases the hybridization of Fe 3d–Se 4p/Te 5p. Based on comparison of Se and Te K-edges, charge transfer between Se and Te is expected: as Te is doped into tetragonal FeSe crystals, the number of 4p holes is increased by Fe 3d–Se 4p/Te 5p hybridization. These results are consistent with the earlier study of the structural distortion that is associated with variation in the angle γ and electron-transport properties.[29] The change in the number of p holes between Fe–Se and Fe–Te may determine superconducting behavior.

Te doping causes structural distortions in FeSe, as revealed by detailed X-ray refinement.[29] Doping expands the lattice because the ionic radius of Te exceeds that of Se. As the doping concentration increases, angle γ varies, increasing the bond length along the *c*-axis and altering the density of states at the Fermi level,[29] consistent with density-functional calculations.[19] T_c and angle γ follow a similar trend: both reach their maxima at $x = 0.5$. Fig. 6 plots T_c against Te doping (T_c is marked by a red star); a simple sketch of the varying γ angle is also shown. Since there is no significant change in the electronic structure around the Fe site in $FeSe_{1-x}Te_x$, the effect of the Se 4p holes on the superconductivity should be naturally examined. The energy shift or the area under the absorption feature of XAS yields the hole concentration. Therefore, the energy shift with respect to pure FeSe was determined from the Se K-edge of $FeSe_{1-x}Te_x$, and is presented in Fig. 6 as a black circle. The evolution of the edge shift provides a reasonable estimate of the hole concentration. The variation in the number of Se 4p holes is closely related to the change in transition temperature. The correlation between the Se 4p hole concentration and T_c suggests that T_c depends more strongly on the variation in the number of 4p holes than on the Fe–Fe interaction in the Fe plane, which claim is consistent with the absence of a significant change in the Fe XAS and RIXS. It is also consistent with the asymmetric expansion of the tetragonal lattice in relation to the structure of $FeSe_{0.5}Te_{0.5}$—by 8% along the *c*-axis but only about 0.6% along the *a*-axis,[29] the Fe–Fe interaction in the Fe plane has an insignificant impact herein. In contrast, the role of the ligand holes and, therefore, the effect of charge transfer, are important; these effects may arise from the fact that Fe acts as a superexchange medium, which does not observably change from the point of view of the Fe site, which finding is consistent with previous studies.[30–32] This finding may

provide an important basis for understanding the origin of superconductivity in the family of compounds considered here.

Conclusion

This investigation discussed the electronic properties that are related to the electron correlation and superconductivity of $FeSe_{1-x}Te_x$, with reference to measurements of XAS and RIXS. The spectroscopic data herein exhibit the signature of Fe 3d localization and different hybridization effects from those of "1111" and "122" systems. The variation of T_c correlates well with the structural deformation and the change in the Se 4p holes. The change of the number of ligand 4p holes may arise from charge transfer between Se and Te. An analysis indicates that the superconductivity in Fe-based compounds of this class is strongly associated with the ligand 4p hole state. The spectral results further indicate that $FeSe_{1-x}Te_x$ is unlikely to be a weakly correlated system like the "1111" and "122" Fe–pnictides. Much remains to be learned about this class of materials. A fundamental question concerning the role of Fe magnetism in these superconductors is yet to be answered, and the importance of charge transfer and the ligand 4p hole state should also be considered. Tetragonal FeSe with a PbO structure not only has the same planar sublattice as layered Fe-based quaternary oxypnictides but also exhibits a structural stability upon Te substitution; it may therefore be a candidate for determining the origin of T_c in Fe-based superconductors.

Acknowledgements

The authors would like to thank the National Science Council of the Republic of China, Taiwan, for financially supporting this research under Contract Nos. NSC-98-2112- M-213-006-MY3 and NSC-099-2112-M-001-036-MY3. The NSRRC staff is appreciated for its valuable discussions and experimental support. The Advanced Light Source is supported by the Director, Office of Science, Office of Basic Energy Sciences of the U.S. Department of Energy, under Contract No. DE-AC02-05CH11231.

References

1 Y. Kamihara, T. Watanabe, M. Hirano and H. Hosono, *J. Am. Chem. Soc.*, 2008, **130**, 3296.
2 C. de la Cruz, Q. Huang, J. W. Lynn, J. Li, W. Ratcliff II, J. L. Zarestky, H. A. Mook, G. F. Chen, J. L. Luo, N. L. Wang and P. Dai, *Nature*, 2008, **453**, 899.
3 G. Xu, W. M. Ming, Y. G. Yao, X. Dai, S. C. Zhang and Z. Fang, *Europhys. Lett.*, 2008, **82**, 67002.
4 F. C. Hsu, J. Y. Luo, K. W. Yeh, T. K. Chen, T. W. Huang, P. M. Wu, Y. C. Lee, Y. L. Huang, Y. Y. Chu, D. C. Yan and M. K. Wu, *Proc. Natl. Acad. Sci. U. S. A.*, 2008, **105**, 14262.
5 B. H. Mok, S. M. Rao, M. C. Ling, K. J. Wang, C. T. Ke, P. M. Wu, C. L. Chen, F. C. Hsu, T. W. Huang, J. Y. Luo, D. C. Yan, K. W. Yeh, T. B. Wu, A. M. Chang and M. K. Wu, *Cryst. Growth Des.*, 2009, **9**, 4847.
6 F. Ma, W. Ji, J. Hu, Z. Y. Lu and T. Xiang, *Phys. Rev. Lett.*, 2009, **102**, 177003.
7 W. L. Yang, A. P. Sorini, C.-C. Chen, B. Moritz, W.-S. Lee, F. Vernay, P. Olalde-Velasco, J. D. Denlinger, B. Delley, J.-H. Chu, J. G. Analytis, I. R. Fisher, Z. A. Ren, J. Yang, W. Lu, Z. X. Zhao, J. van den Brink, Z. Hussain, Z.-X. Shen and T. P. Devereaux, *Phys. Rev. B: Condens. Matter Mater. Phys.*, 2009, **80**, 014508.
8 A. Tamai, A. Y. Ganin, E. Rozbicki, J. Bacsa, W. Meevasana, P. D. C. King, M. Caffio, R. Schaub, S. Margadonna, K. Prassides, M. J. Rosseinsky and F. Baumberger, *Phys. Rev. Lett.*, 2010, **104**, 097002.
9 B. C. Sales, A. S. Sefat, M. A. McGuire, R. Y. Jin, D. Mandrus and Y. Mozharivskyj, *Phys. Rev. B: Condens. Matter Mater. Phys.*, 2009, **79**, 094521.
10 M. Aichhorn, L. Pourovskii, V. Vildosola, M. Ferrero, O. Parcollet, T. Miyake, A. Georges and S. Biermann, *Phys. Rev. B: Condens. Matter Mater. Phys.*, 2009, **80**, 085101.
11 K. Nakayama, T. Sato, P. Richard, T. Kawahara, Y. Sekiba, T. Qian, G. F. Chen, J. L. Luo, N. L. Wang, H. Ding and T. Takahashi, *Phys. Rev. Lett.*, 2010, **105**, 197001.
12 D. Arčon, P. Jeglič, A. Zorko, A. Potočnik, A. Y. Ganin, Y. Takabayashi, M. J. Rosseinsky and K. Prassides, *Phys. Rev. B: Condens. Matter Mater. Phys.*, 2010, **82**, 140508(R).
13 K. W. Yeh, C. T. Ke, T. W. Huang, T. K. Chen, Y. L. Huang, P. M. Wu and M. K. Wu, *Cryst. Growth Des.*, 2009, **9**, 4847.
14 J. Norgdren, G. Bray, S. Cramm, R. Nyholm, J. E. Rubensson and N. Wassdahl, *Rev. Sci. Instrum.*, 1989, **60**, 1690.
15 F. Bondino, E. Magnano, M. Malvestuto, F. Parmigiani, M. A. McGuire, A. S. Sefat, B. C. Sales, R. Jin, D. Mandrus, E. W. Plummer, D. J. Singh and N. Mannella, *Phys. Rev. Lett.*, 2008, **101**, 267001.
16 I. A. Nekrasov, Z. V. Pchelkina and M. V. Sadovskii, *JETP Lett.*, 2008, **88**, 144.
17 L. C. Duda, J. Nordgren, G. Drager, S. Bocharov and T. Kirchner, *J. Electron Spectrosc. Relat. Phenom.*, 2000, **110**, 275.
18 S. Raghu, X. L. Qi, C. X. Liu, D. J. Scalapino and S. C. Zhang, *Phys. Rev. B: Condens. Matter Mater. Phys.*, 2008, **77**, 220503(R).
19 A. Subede, L. Zhang, D. J. Singh and M. H. Du, *Phys. Rev. B: Condens. Matter Mater. Phys.*, 2008, **78**, 134514.
20 A. Yamasaki, S. Imada, K. Takase, T. Muro, T. Kato, H. Kobori, A. Sugimura, N. Umeyama, H. Sato, Y. Hara, N. Miyakawa and S. I. Ikeda, arXiv: 0902.3314v3, 2009.
21 M. Aichhorn, S. Biermann, T. Miyake, A. Georges and M. Imada, *Phys. Rev. B: Condens. Matter Mater. Phys.*, 2010, **82**, 064504.
22 B. Freelon, T. S. Lir, X. R. Rotundu, S. D. Wilson, J.-H. Guo, J. L. Chen, W. L. Yang, C. L. Chang, P. A. Glans, P. Shirage, A. Iyo and R. J. Birgeneau, *J. Phys. Soc. Jpn.*, 2010, **79**, 074716.
23 E. Z. Kurmaev, J. A. McLeod, A. Buling, N. A. Skorikov, A. Moewes, M. Neumann, M. A. Korotin, Yu. A. Izyumov, N. Ni and P. C. Canfield, *Phys. Rev. B: Condens. Matter Mater. Phys.*, 2009, **80**, 054508.
24 G. A. Sawatzky, J. Zaanen and J. W. Allen, *Phys. Rev. Lett.*, 1985, **55**, 418.
25 P. G. Steeneken, L. H. Tjeng, G. A. Sawatzky, A. Tanaka, O. Tjernberg, G. Ghiringhelli, N. B. Brookes, A. A. Nugroho and A. A. Menovsky, *Phys. Rev. Lett.*, 2003, **90**, 247005.
26 C. L. Chen, S. M. Rao, C. L. Dong, J. L. Chen, T. W. Huang, B. H. Mok, M. C. Ling, W. C. Wang, C. L. Chang, T. S. Chan, J. F. Lee, J.-H. Guo and M. K. Wu, *Europhys. Lett.*, 2011, **93**, 47003.
27 B. Joseph, A. Iadecola, L. Simonelli, Y. Mizuguchi, Y. Takano, T. Mizokawa and N. L. Saini, *Phys. Rev. B: Condens. Matter*, 2010, **22**, 485702.
28 B. Joseph, A. Iadecola, A. Puri, L. Simonelli, Y. Mizuguchi, Y. Takano and N. L. Saini, *Phys. Rev. B: Condens. Matter Mater. Phys.*, 2010, **82**, 020502(R).
29 K. W. Yeh, Z. W. Huang, Y. L. Huang, T. K. Chen, F. C. Hsu, P. M. Wu, Y. C. Lee, Y. Y. Chu, C. L. Chen, J. Y. Luo, D. C. Yan and M. K. Wu, *Europhys. Lett.*, 2008, **84**, 37002.
30 M. H. Fang, H. M. Pham, B. Qian, T. J. Liu, E. K. Vehstedt, L. Spinu and Z. Q. Mao, *Phys. Rev. B: Condens. Matter Mater. Phys.*, 2008, **78**, 224503.
31 T. Yildrim, *Phys. Rev. Lett.*, 2008, **101**, 057010.
32 Q. Si and E. Abrahams, *Phys. Rev. Lett.*, 2008, **101**, 076401.

